

Removal of anionic (Acid Yellow 17 and Amaranth) dyes using aminated avocado (*Persea americana*) seed powder: adsorption/desorption, kinetics, isotherms, thermodynamics, and recycling studies

Venkata Subbaiah Munagapati, Hsin-Yu Wen, Yarramuthi Vijaya, Jet-Chau Wen, Jhy-Horng Wen, Zhong Tian, Guda Mallikarjuna Reddy & Jarem Raul Garcia

To cite this article: Venkata Subbaiah Munagapati, Hsin-Yu Wen, Yarramuthi Vijaya, Jet-Chau Wen, Jhy-Horng Wen, Zhong Tian, Guda Mallikarjuna Reddy & Jarem Raul Garcia (2021) Removal of anionic (Acid Yellow 17 and Amaranth) dyes using aminated avocado (*Persea americana*) seed powder: adsorption/desorption, kinetics, isotherms, thermodynamics, and recycling studies, International Journal of Phytoremediation, 23:9, 911-923, DOI: [10.1080/15226514.2020.1866491](https://doi.org/10.1080/15226514.2020.1866491)

To link to this article: <https://doi.org/10.1080/15226514.2020.1866491>



Published online: 06 Jan 2021.



Submit your article to this journal [↗](#)



Article views: 80



View related articles [↗](#)



View Crossmark data [↗](#)



Citing articles: 1 View citing articles [↗](#)



Removal of anionic (Acid Yellow 17 and Amaranth) dyes using aminated avocado (*Persea americana*) seed powder: adsorption/desorption, kinetics, isotherms, thermodynamics, and recycling studies

Venkata Subbaiah Munagapati^a, Hsin-Yu Wen^b, Yarramuthi Vijaya^c, Jet-Chau Wen^{a,d}, Jhy-Horng Wen^e, Zhong Tian^f, Guda Mallikarjuna Reddy^{g,h}, and Jarem Raul Garcia^h

^aResearch Centre for Soil and Water Resources and Natural Disaster Prevention (SWAN), National Yunlin University of Science and Technology, Douliou, Taiwan; ^bDepartment of Pathology, West China Hospital, Sichuan University, Chengdu, PR China; ^cDepartment of Chemistry, Vikrama Simhapuri University, Nellore, India; ^dDepartment of Safety, Health, and Environmental Engineering, National Yunlin University of Science and Technology, Douliou, Taiwan; ^eDepartment of Electrical Engineering, Tunghai University, Taichung, Taiwan; ^fState Key Laboratory of Hydraulics and Mountain River Engineering, Sichuan University, Chengdu, PR China; ^gChemical Engineering Institute, Ural Federal University, Yekaterinburg, Russia; ^hDepartment of Chemistry, State University of Ponta Grossa, Ponta Grossa, Brazil

ABSTRACT

Aminated avocado seed powder (AASP)—an eco-friendly novel adsorbent has been used for the removal of Acid Yellow 17 (AY 17) and Amaranth (AMR) from an aqueous phase. The AASP (before and after adsorption) was systematically characterized by different analytical techniques such as FT-IR, FESEM, EDX, and N₂ adsorption-desorption analysis. Non-linear form of various kinetic (PFO and PSO) and isotherm (Langmuir and Freundlich) models were used to examine the adsorption behavior of AY 17 and AMR onto AASP. The adsorption of AY 17 and AMR onto AASP was well illustrated by the PSO kinetic model and Langmuir isotherm models. At 303 K, the maximum adsorption capacities (obtained from the Langmuir) of the AASP for AY 17 and AMR was 42.7 and 89.2 mg/g, respectively. The AY 17 and AMR adsorption was strongly pH-dependent with an optimum pH value of 2.0. Activation energy was calculated as 12.3 and 16.3 kJ/mol for AY 17 and AMR respectively, suggesting physical adsorption. The positive values of ΔG° and ΔH° indicated that the adsorption process of AY 17 and AMR onto AASP was non-spontaneous and endothermic. The negligible loss of adsorption capacity and excellent regeneration of AASP were observed for the five cycles.

Statement of novelty: The present research majorly focused on the synthesis of adsorbent from Avocado seed for the removal of Acid Yellow 17 and Amaranth anionic dyes from aqueous solution. Although the literature is available on direct seed powder as adsorbent, to the best of our knowledge, no chemical modified adsorbent synthesis was not available. Hence, to fill the gap in the literature, we chose the following study that significantly enhanced the adsorption efficiency of the selected anionic dyes.

KEYWORDS

Adsorption; anionic dyes; isotherms; kinetics; thermodynamics

Introduction

Water pollution is a major environmental threat that needs immediate attention. Industrial wastes are significant contributors to the surface as well as groundwater contamination and pollution. The effluents from textile, paper printing, cosmetics, leather, dyestuff, and plastic industries carry large quantities of dye-contaminated water that is very difficult to undergo natural biochemical degradation. This is due to its complex composition, high toxicity, variable pH ranges, dark color, and strong odor. These factors are adversely affecting the aquatic life, and dysregulating the self-purification of water using the natural microbiota. This is also interfering with the biological water cycle of nature, leading to toxicity to humans. Toxicity and carcinogenicity

are the principal effects on human beings (Albadarin *et al.* 2014; Adeyemo *et al.* 2017; Yaseen and Scholz 2018). Therefore, there is an urgent need to remove toxic dyes from wastewater before the release into the environment.

Acid Yellow 17 (AY 17) and Amaranth (AMR) are highly water-soluble anionic dyes, which are widely used for coloring textile materials, paper, carpet, wood, and leather, etc., and during these processes, excess dye enters into the wastewater. These dyes cause many adverse health effects such as irritation to eyes, tumors, birth effects, respiratory problems, high genotoxicity, cytostaticity, cytotoxicity, mutagenicity, and carcinogenicity (Ashraf *et al.* 2013; Njoku *et al.* 2014; Guerrero-Coronilla *et al.* 2015; Liao and Wang 2018). Therefore, from an environmental, and safety perception,

the removal of AY 17 and AMR from wastewater before their discharge is an important task. There are several conventional physicochemical treatment technologies, such as coagulation/flocculation (Saritha *et al.* 2017), photodegradation (Roşu *et al.* 2016), advanced oxidation process (Nidheesh *et al.* 2018), ion exchange (Ma *et al.* 2019), membrane filtration (Qi *et al.* 2019), chemical oxidation/reduction (Li *et al.* 2014), adsorption (Munagapati *et al.* 2019), etc., have been developed and successfully applied to remove the dye contaminants from the wastewater. However, each of these techniques has several disadvantages, such as very harsh reaction conditions, low efficiency, high expensive, incomplete removal, generation of harmful substances, and time-consuming. Among the physicochemical methods, adsorption has been considered as an attractive and useful technique due to its cost-effectiveness, high efficiency even in low dye concentration, ease of operation, the possibility to recover, and reuse the adsorbents and broadly applicable process.

Agricultural waste material has a potential role in the treatment of wastewaters which can eliminate different dyes (Gündüz and Bayrak 2017; Kamranifar *et al.* 2018; Munagapati *et al.* 2018; Stavrinou *et al.* 2018; Çelekli *et al.* 2019). Using these materials as adsorbent has dual benefits, this can save the disposal costs of these materials and at the same time reducing the threat to the environment. Moreover, these materials are composed of lignocellulosic compounds, *i.e.*, lignin, hemicellulose, and cellulose which are known to support the adsorption phenomenon (Chen *et al.* 2011). *Persea americana*, commonly known as avocado, is a tropical fruiting tree with edible flesh, and a non-edible seed. These seeds are usually considered waste and get discarded. However, like other plant residues, avocado seeds are mainly composed of hemicellulose, cellulose, and lignin making this a good source for the development and production of new low-cost adsorbent compounds that can be used in the water treatment processes. In recent years, many research teams have focused on improving the adsorption performance of inexpensive adsorbent materials through physical or chemical modifications. These modifications used to sorbents may introduce functional groups (hydroxyl, carboxylate, amine, phosphonate, amide, sulfonate, etc.) in the surface of the sorbents or increase their porosity, with an increase in their adsorption efficiency. Though, there are distinct chemical modifications have been done to various agricultural waste materials and newly synthesized adsorbents such as cationic modified orange peel powder (Munagapati and Kim 2016), base-modified *Artocarpus odoratissimus* leaves (Zaidi *et al.* 2019), sulfuric acid-treated orange peel (Senthil Kumar *et al.* 2014), spent tea leaves modified with polyethyleneimine (Wong *et al.* 2019), chemically modified garlic peels (Zhao *et al.* 2019), phosphoric acid modified orange peel (Guediri *et al.* 2020), chemically modified *Luffa aegyptica* peel (Mashkoo and Nasar 2019), acid-washed black cumin seed powder (Siddiqui *et al.* 2018), chemically modified banana peel powder (Munagapati *et al.* 2020), and treated watermelon seeds (Benkaddour *et al.* 2018) were successfully utilized for the

removal of different dyes. In the present study, aminated avocado seed powder (AASP) was taken as adsorbent material for the removal of AY 17, and AMR from the aqueous phase.

In this context, the objective of this paper, we used the AASP as an adsorbent to remove AY 17 and AMR from aqueous system. The influence of different parameters, such as solution pH, initial dye concentration, contact time, and temperature was examined. The adsorption mechanism of AY 17 and AMR onto AASP was derived by studying the isotherms, kinetics and thermodynamics studies. Similarly, reusability potential of AASP was identified by studying adsorption-desorption cycles.

Materials and methods

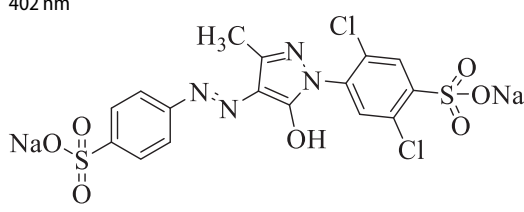
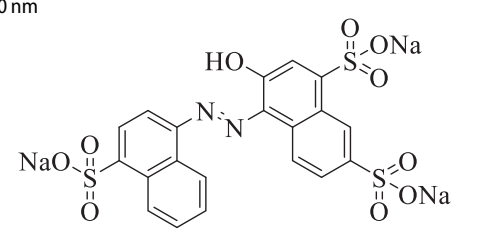
Materials

In this study, all reagents used were of analytical grade and were used without any further purification. AY 17, AMR, ethanolamine (HOCH₂CH₂NH₂), hydrochloric acid (HCl), sodium hydroxide (NaOH), sulfuric acid (H₂SO₄), nitric acid (HNO₃), sodium chloride (NaCl), and sodium carbonate (Na₂CO₃) were procured from Sigma-Aldrich Co., Taiwan. A 1,000 mg/L stock solution (of both dyes) and working solutions for adsorption experiments were prepared in double-deionized water (DDW). The general characteristics of both dyes are listed in Table 1.

Preparation of AASP

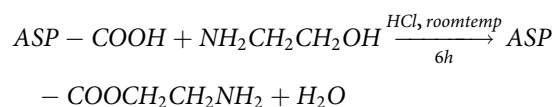
Avocado seeds (AS) were collected from a local fruit market in Taiwan. The seeds were cut into small pieces after

Table 1. Characteristics of AY 17 and AMR.

AY 17	
Molecular formula	C ₁₆ H ₁₀ Cl ₂ N ₄ Na ₂ O ₇ S ₂
Molecular weight	551.29 g/mol
Dye content	60%
λ _{max}	402 nm
Structure	
AMR	
Molecular formula	C ₂₀ H ₁₁ N ₂ Na ₃ O ₁₀ S ₃
Molecular weight	604.47 g/mol
Dye content	85%
λ _{max}	520 nm
Structure	

washing under tap water until impurities were gone and dried in sunlight. The sun-dried seeds were crushed and ground into a fine powder and sieved to 0.5 mm (35 mesh) particle size. After that, the powder was washed with DDW, and dried in a vacuum oven at 343 K for 24 h, then boiled in DDW by changing the water frequently until the water becomes colorless, which shows the removal of water-soluble color materials. Then, the obtained powder was oven-dried at 353 K for 24 h. This treated powder names as ASP.

The aminated adsorbent was prepared according to the previously reported method (Subbaiah and Kim 2016). Firstly, 5.0 g of ASP was added with 100 mL of HOCH₂CH₂NH₂ and 20.8 mL of Con. HCl. The reaction mixture was agitated on a thermostatic shaker (150 rpm) at 298 K for 6 h. The reaction occurs as follows:



After agitation, the treated ASP was collected by centrifugation and was sequentially washed with DDW. The treated ASP was dried in a convection oven at 343 K for 24 h for complete dryness, and the resultant final ASP was named as AASP.

Characterization

The morphological characteristics of AASP (before and after dyes sorption) were studied by using FESEM (JEOL JSM-6701F, Japan) after gold metallization. The instrument is combined with an EDX analyzer. The textural properties of the AASP were determined by adsorption/desorption of N₂ at 77 K using surface area analyzer (Quantachrome Autosorb IQ, USA) with liquid nitrogen. Before N₂ sorption measurement, the sample was degassed at 473 K for 6 h. The N₂ adsorption on the sample was used to calculate the specific surface area through the BET equation. The pore size distribution and pore volume were evaluated using the BJH model. The amount of gas adsorbed at a relative pressure of ($P/P_o = 0.995$) was used to calculate pore volume. The surface functional groups of AASP during the adsorption process (before and after dyes adsorption) were identified by FT-IR spectrometer (Perkin-Elmer Spectrum Two, USA). The samples were prepared by KBr pellets technique (1:10, sample with KBr) and the scan spectral range was 4,000–400 cm⁻¹.

Point of zero charge (pH_{pzc})

The pH_{pzc} of the AASP was determined using the solid addition method (Silva *et al.* 2013). For this purpose, 30 mL of 0.1 M KNO₃ solution was taken in a series of 50 mL glass vial bottles, and pH of each solution was adjusted from 0.2 to 10.0 by using 0.1 M NaOH or HCl solutions. The initial pH of these solutions was noted as pH_i using pH meter (Mettler Toledo, USA). After that, 50 mg of AASP was added to each bottle, and these bottles were placed on a

thermostatic shaker were agitated at 180 rpm for 24 h until equilibrium is established. Afterwards, the final pH in each suspension was read as pH_f and pH_{pzc} value was determined from the plot of pH_i-pH_f (ΔpH) versus pH_i. The intersection point of the axis passing through zero and the resulting curve gives the value of the pH_{pzc}.

Batch adsorption studies

The batch mode experiments were performed to study the adsorption of AY 17 and AMR onto AASP. For pH experiments, 50 mg of AASP adsorbent was added to 30 mL of dye solutions (300 mg/L) taken in 50 mL of glass vial bottles. Before adding with the AASP, different pH values (2.0–10.0) of both dye solutions was controlled by adding HCl (0.1 M) or NaOH (0.1 M). Kinetics was studied by adding 50 mg of AASP with 30 mL of dye solutions (300 mg/L, pH 2.0), followed by adsorption process at various temperatures (303, 313, and 323 K) in a time interval of 0–240 min. The adsorption isotherms at pH 2.0 were studied at different (100–1,000 mg/L) initial concentration of AY 17 and AMR solutions. The thermodynamic study was carried out at three various temperatures maintaining the other parameters as said above. In all experiments, the suspensions were then placed in a temperature-controlled thermostatic reciprocating shaker and agitated at a constant speed of 180 rpm. At the end of each experiment, 10 mL of the solution samples were withdrawn at a predetermined time and separate the clear supernatant using a centrifuge at 5,000 rpm for 10 min. The absorbance after AY 17 and AMR adsorption was measured by using a UV-Vis spectrometer. The average value (duplicate results of all the experiments) was used for calculations.

The adsorption capacity q_e , along with the percentage of dye removal (%), were measured by using the following equations, respectively.

$$q_e(\text{mg/g}) = \frac{[C_o(\text{mg/L}) - C_e(\text{mg/L})]V(L)}{M(\text{g})} \quad (1)$$

$$\text{Removal}(\%) = \frac{(C_o - C_e)}{C_o} \times 100 \quad (2)$$

Desorption studies

The desorption studies were conducted under optimal conditions obtained from adsorption studies in batch method. Briefly, 50 mg of AASP was mixed to the solution containing 30 mL of 300 mg/L of both dyes for 120 min under 180 rpm at 303 K. After that, the dye-loaded AASP samples were centrifuged at 6,000 rpm for 10 min for separation. The samples were dried in an oven at 343 K for 6 h. Then, saturated AASP samples were treated with 30 mL of 0.1 M NaOH, NaCl, Na₂CO₃, HCl, HNO₃, and H₂SO₄ to elute both dyes from the surface of AASP. The desorption efficiency of dye was calculated according to the following

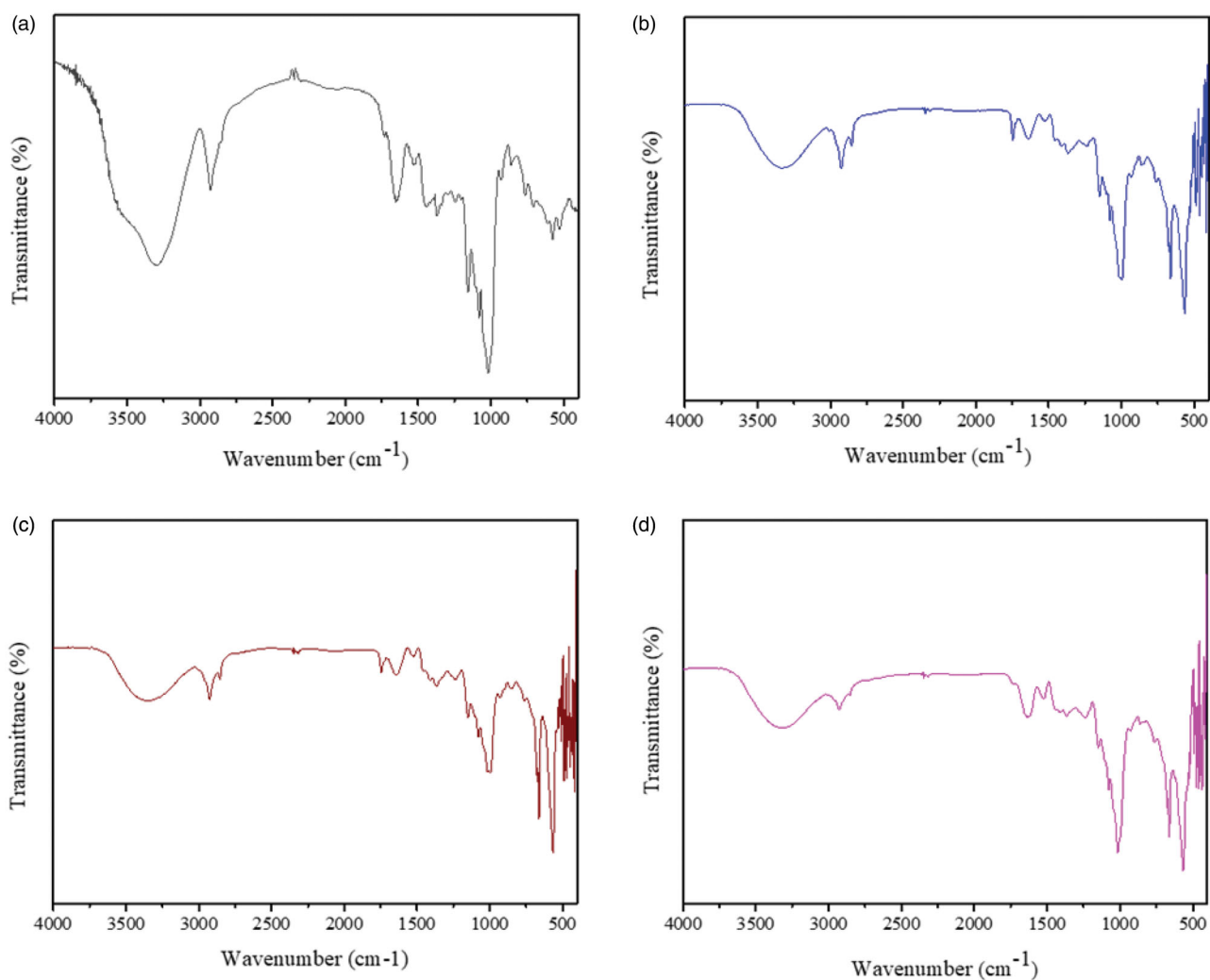


Figure 1. FTIR spectra of (a) raw ASP; (b) unadsorbed AASP; (c) AY 17 adsorbed AASP; and (d) AMR adsorbed AASP.

Equation (3):

$$\text{Desorption efficiency} = \frac{\text{Amount of dye desorbed}}{\text{Amount of dye adsorbed}} \times 100 \quad (3)$$

Error analysis

The Chi-square (χ^2) test was applied to compare experimental data and predictions from the non-linear Langmuir and Freundlich isotherm models. χ^2 is used to find the consistency of the data obtained from the model with the experimental data. The equivalent mathematical statement of χ^2 test can be defined as:

$$\chi^2 = \sum_{i=1}^n \left(\frac{(q_{e, \text{exp}} - q_{e, \text{cal}})^2}{q_{e, \text{cal}}} \right) \quad (4)$$

Results and discussion

Characterization

FT-IR analysis indicates the functional groups present on the adsorbent surface. Figure 1 displays the FT-IR spectra of

the raw ASP, unloaded AASP, AY 17-loaded AASP, and AMR-loaded AASP. Figure 1a shows a strong peak at $3,301 \text{ cm}^{-1}$ might be attributed to the N-H or O-H stretching vibrations. The peak at $2,931 \text{ cm}^{-1}$ was assigned for -C-H stretching vibrations in -CH and -CH₂ groups. The peak at $1,737 \text{ cm}^{-1}$ could be assigned to C=O stretching vibrations of the carboxyl group. The bands at $1,649$ and $1,441 \text{ cm}^{-1}$ were attributed to the stretching vibration of C=O groups. The peak at $1,529 \text{ cm}^{-1}$ is due to -C-O or C=C stretching vibrations. The band at $1,372 \text{ cm}^{-1}$ may be assigned to -C-H bending of the alkyl group. The peaks at $1,154$ and $1,021 \text{ cm}^{-1}$ correspond to the -C-H stretching and C-O-H bending vibrations. The spectrum of AASP (Figure 1b) revealed the presence of several peaks ($3,343$, $2,923$, $2,850$, $1,743$, $1,638$, $1,636$, $1,523$, $1,434$, $1,367$, $1,239$, $1,148$, $1,075$, 992 , 855 , 659 , and 559 cm^{-1}) related to different functional groups (hydroxyl, amine, carboxyl, and carbonyl) on the AASP surface. The strong peak around $3,343 \text{ cm}^{-1}$ correspond to the overlapping of -OH (hydroxyl) and -NH (amine) stretching vibration of the adsorbed water. The two bands at $2,923$ and $2,850 \text{ cm}^{-1}$ were due to the -C-H stretching of the alkane functional groups. The band appearing at $1,743 \text{ cm}^{-1}$ was attributed to

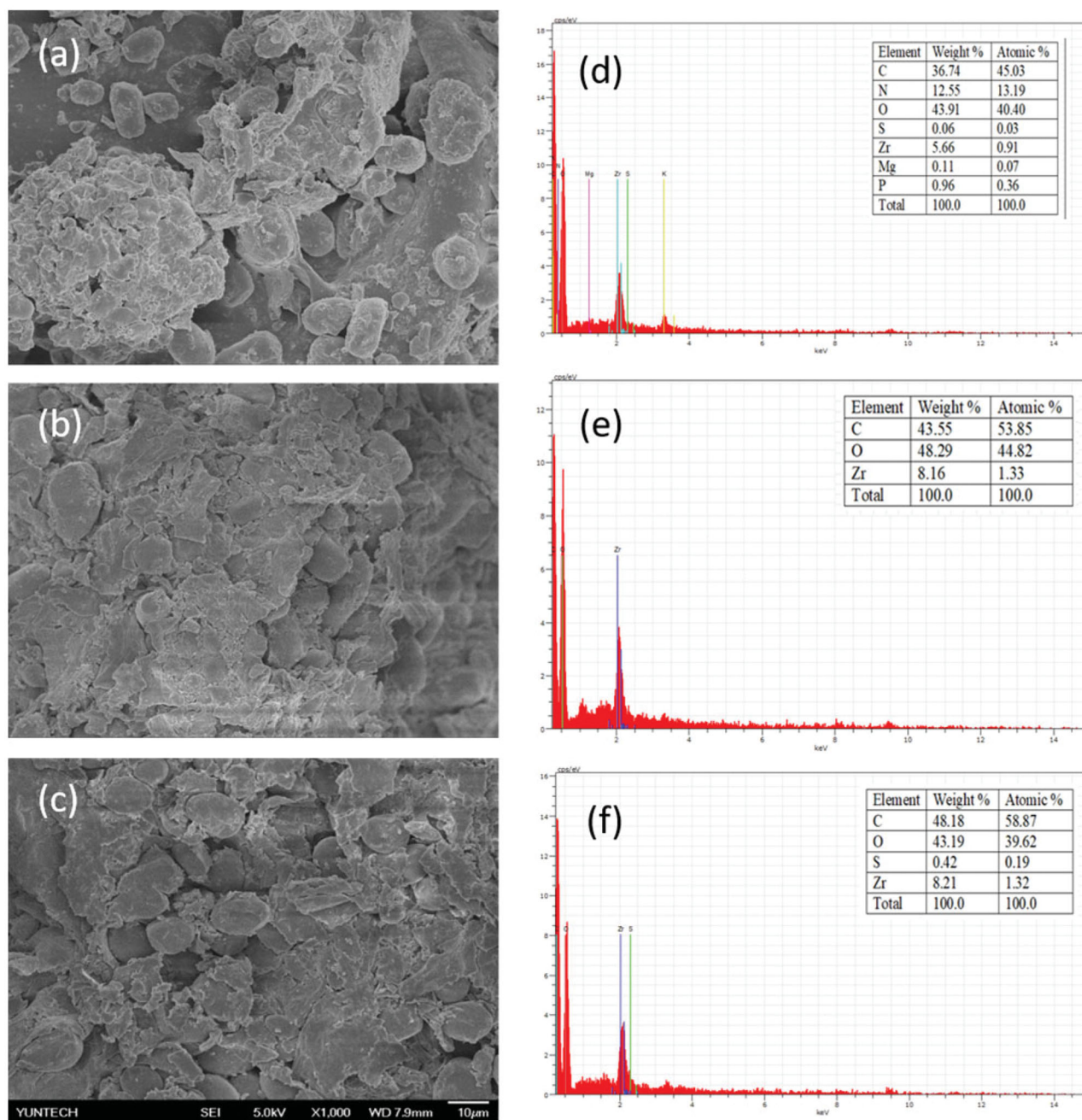


Figure 2. SEM images of: (a) unadsorbed AASP; (b) AY 17 adsorbed AASP; and (c) AMR adsorbed AASP; EDX images of (d) unadsorbed AASP; (e) AY 17 adsorbed AASP; and (f) AMR adsorbed AASP.

the -C=O stretching vibration of the ester group. The sharp adsorption peaks about $1,638$ and $1,523\text{ cm}^{-1}$ were attributed to the C=O , and -NH bonds of amine groups. The band at $1,434\text{ cm}^{-1}$ can be attributed to C-O bending vibration of the alkyl group. The peak at $1,367\text{ cm}^{-1}$ may be assigned to C-N stretching vibrations of the amine group. The peak at $1,239\text{ cm}^{-1}$ was assigned for the C-O stretching frequency. The peaks at $1,148$ and $1,075\text{ cm}^{-1}$ corresponded to the stretching vibrations of C-O-C , and C-O bonds. Bending vibration of -OH groups, stretching vibration of C-H , and C-O bonds were shown between 400 and $1,000\text{ cm}^{-1}$. After modification, the new peaks ($2,850$, $1,239$ and $1,076\text{ cm}^{-1}$) were observed in the AASP spectrum

(Figure 1b). The AY 17 and AMR saturated AASP spectra's (Figure 1c,d) clearly indicate that some peaks are slightly decreasing from their positions and shifting in band intensity after adsorption of AY 17 and AMR. The change in peak positions indicates the involvement of the respective groups during the adsorption of AY 17 and AMR onto AASP.

FESEM-EDX was used to analyze the surface morphology and elemental composition of the adsorbent. Figure 2 shows the SEM micrographs and their respective EDX spectra of AASP before and after AY 17 and AMR adsorption. From Figure 2a, the surface of AASP was irregular, rough and heterogeneous that allows the higher residence time for the

interactions, thereby enhancing the adsorption capacity. After AY 17 and AMR adsorption (Figure 2b,c), the surface of AASP was entirely covered with AY 17 and AMR indicating successful loading on AASP surface. The EDX spectrum

of AASP displays (Figure 2d) the following elements C, N, O, S, Zr, Mg, and P before adsorption. However, after adsorption, some of the elements actively participate in the adsorption phenomenon that leads to the disappearance of some elements while the others are enhanced (see Figure 2e,f). This observation confirmed the loading of the AY 17 and AMR molecules on the surface of the AASP.

Based on BET surface area one can determine the sorption capacity of an adsorbent. There is a directly proportional relationship with the surface area in BET measurements to the availability of a number of vacancies on the surface. Figure 3a displays the N₂ adsorption-desorption equilibrium isotherms of the prepared AASP at 77 K. As we can see in Figure 3a, BET isotherm displays an IV-type (according to the IUPAC classifications) with a hysteresis loop of H₃-type from about P/P₀ = 0.4 to 0.99, which indicates the existence of a mesoporous structure (Hamza *et al.* 2018). The surface area, pore volume, and pore diameter determined by the BET, and BJH methods were 13.9 m²/g, 0.01179 cm³/g, and 1.9127 nm, respectively. The distribution of pore volume concerning the pore diameter of AASP is shown in Figure 3b. The pore size distribution of the AASP ranged between 2.0 and 100 nm. However, the major pore volume was

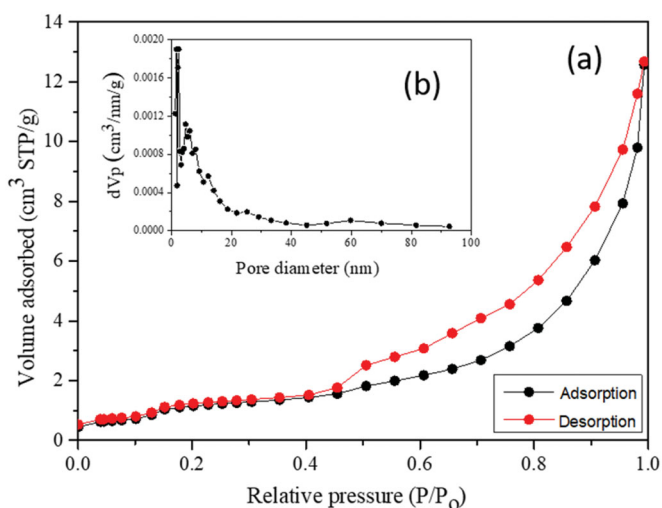


Figure 3. (a) N₂ adsorption-desorption isotherm of the AASP; and (b) pore size distribution of AASP obtained through BJH method.

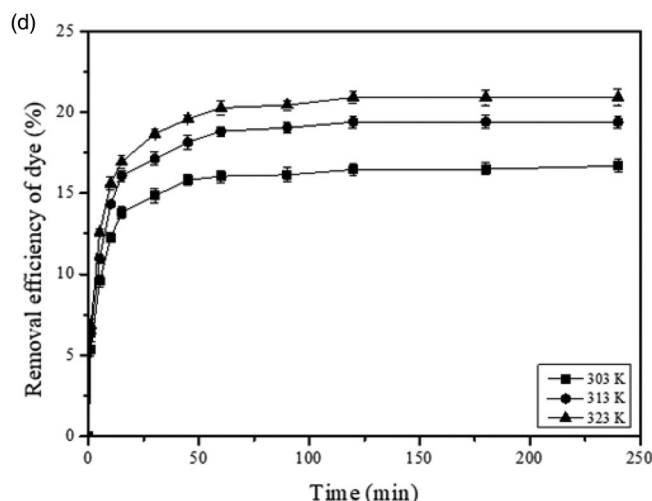
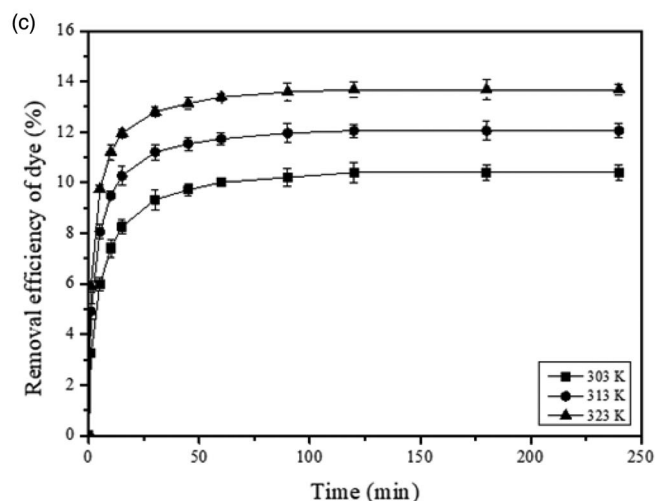
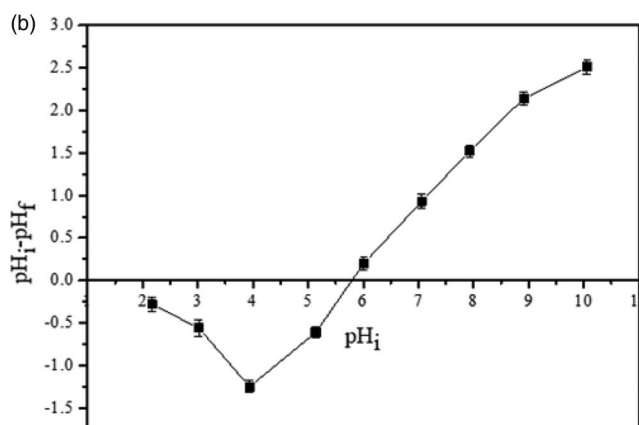
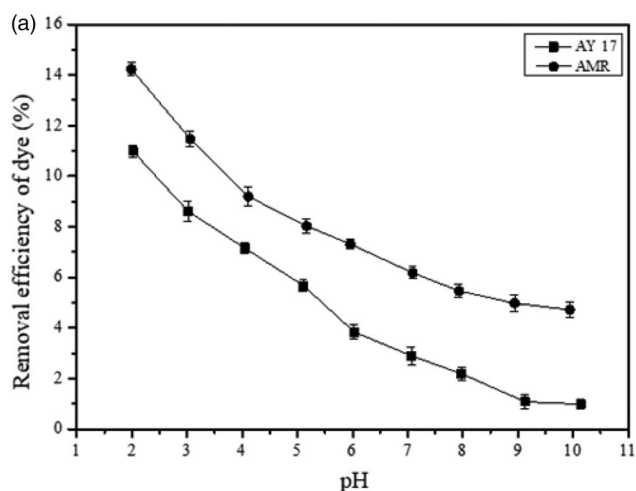


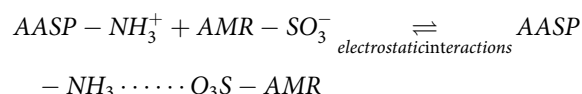
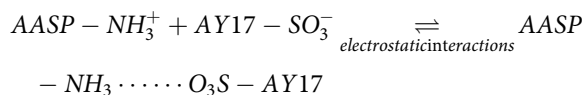
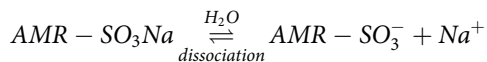
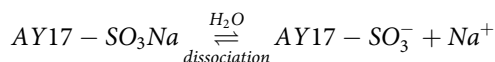
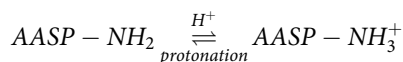
Figure 4. Effect of (a) pH (initial dye concentration: 300 mg/L, volume: 30 mL, agitation: 180 rpm, dose: 50 mg, time: 120 min, temperature: 303 K); (b) point of zero charge of AASP (pH range: 2.0–10.0, electrolyte volume: 30 mL, dose: 50 mg, agitation: 180 rpm, temperature: 303 K); and contact time on the adsorption of (c) AY 17; and (d) AMR onto AASP (initial dye concentration: 300 mg/L, volume: 30 mL, agitation: 180 rpm, pH: 2.0, dose: 50 mg, temperature: 303 K).

contributed by pores with a diameter of 2.0–10 nm. This is in accordance with the mesoporous nature of the AASP as shown from IV-type isotherm (Figure 3a) because in the mesoporous type of isotherms the range of diameter lies between 2.0 to 50 nm (Banerjee *et al.* 2019; Mahmoud *et al.* 2020).

Effect of pH

The pH factor determines the protonation/deprotonation of adsorbates and changes in the surface charges of adsorbents, so this is a vital factor in the sorption process. The effects of pH on the adsorption of AY 17 and AMR onto AASP were studied in the pH range of 2.0–10.0 and results are displayed in Figure 4a. With the increase of pH from 2.0 to 10.0, the removal efficiency decreased from 10.98% to 0.98% for AY 17, and from 14.23% to 4.72% for AMR. The adsorption of AY 17 and AMR strongly dependent on pH and around pH 2.0 the maximum adsorption was found. The pH_{pzc} value of the AASP was observed at 5.8 (Figure 4b) when the solution pH is less than pH_{pzc} a positive charge is induced (develops) on its surface on the other hand when the solution pH values are higher than pH_{pzc} the charge decreases (Jiang and Hu 2019). Therefore, when the solution pH is less than pH_{pzc} , the AASP surface was probably with a positive charge. This may be expected due to the protonation of amine groups of AASP by the availability of a huge number of protons in the surrounding solution of AASP. Hence a number of $-NH_3^+$ groups which are nothing but adsorption sites increased on the AASP. On the contrary, the sulfonate group ($-SO_3Na$) present in the molecular structure of adsorbate (AY 17 and AMR) in the aqueous medium behaves like negative sulfonate group ($-SO_3^-$). These will be more active when the AASP behaves as positive charge centers. Consequently, an electrostatic attraction takes place between protonated amino ($-NH_3^+$) group of AASP, and sulfonate ($-SO_3^-$) group of adsorbent (AY 17 and AMR) thus dye adsorption increases.

Adsorption mechanism may be as follows:



When the system pH increases, the increase in negatively charged binding sites is expected. Therefore because of

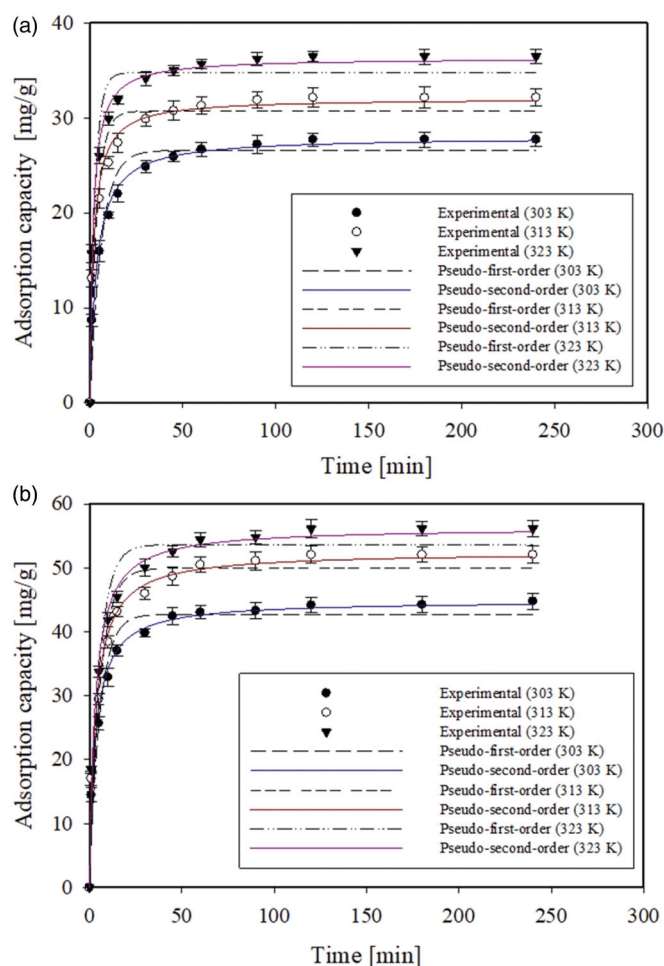


Figure 5. Non-linear kinetic plots for the adsorption of (a) AY 17; and (b) AMR onto AASP (initial dye concentration: 300 mg/L, volume: 30 mL, agitation: 180 rpm, pH: 2.0, dose: 50 mg, temperature: 303–323 K).

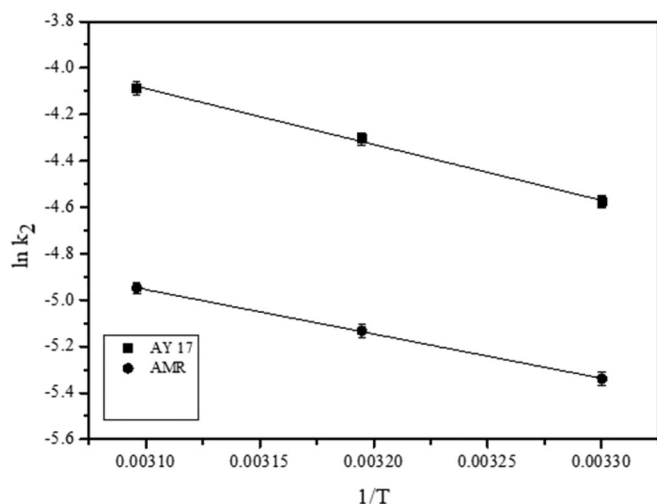
electrostatic repulsions between the same kind of charges, the AASP (negatively charged surface) will not adsorb the adsorbent (AY 17 and AMR) that also has the negative charge. In addition to this at higher pH, an ample concentration of OH^- ions would be expected and these will compete with the adsorbent (AY 17 and AMR) molecules. There is higher competition for the fixed available AASP surface (positively charged) sites. Therefore, this reduces the adsorption efficiency of adsorbent (AY 17 and AMR). The adsorption of AY 17 and AMR was favored at pH solution $< pH_{pzc}$. Hence, the initial pH 2.0 of the AY 17 and AMR solutions was fixed for further adsorption experiments. A similar phenomenon on the effect of pH was observed with respect to the anionic dyes (Kumar *et al.* 2010; Çelekli *et al.* 2012; Bhomick *et al.* 2018; Thirunavukkarasu *et al.* 2018; Hassan *et al.* 2020).

Effect of contact time

Another vital parameter contact time plays a crucial role in determining the adsorption rate as well as the estimation of equilibrium time for the dye adsorption. Figure 4c,d represents the effect of contact time on the adsorption efficiency of AY 17 and AMR onto AASP at different temperatures

Table 2. Kinetic parameters for the adsorption of AY 17 and AMR onto AASP at different temperatures.

Dye	Temp. (K)	$q_{e, exp}$ (mg/g)	Pseudo-first-order model			Pseudo-second-order model		
			$q_{e1, cal}$ (mg/g)	k_1 (1/min)	R^2	$q_{e2, cal}$ (mg/g)	k_2 (g/mg min)	R^2
AY17	303	28.12	23.57 ± 0.66	0.163 ± 0.001	0.9562	27.98 ± 0.72	0.011 ± 0.001	0.9905
	313	33.67	28.71 ± 0.81	0.266 ± 0.001	0.9415	32.04 ± 0.97	0.014 ± 0.002	0.9899
	323	38.42	33.74 ± 0.91	0.354 ± 0.003	0.9479	39.46 ± 1.28	0.017 ± 0.004	0.9931
AMR	303	44.12	36.71 ± 1.02	0.173 ± 0.002	0.9607	44.84 ± 1.75	0.005 ± 0.0001	0.9912
	313	51.32	44.89 ± 1.46	0.177 ± 0.004	0.9571	52.46 ± 2.34	0.006 ± 0.0004	0.9934
	323	55.75	51.59 ± 2.18	0.187 ± 0.007	0.9546	56.23 ± 2.89	0.007 ± 0.0005	0.9915

**Figure 6.** Plots of $\ln k_2$ versus $1/T$ for the estimation of activation energy for the adsorption of AY 17 and AMR onto AASP (initial dye concentration: 300 mg/L, volume: 30 mL, agitation: 180 rpm, pH: 2.0, dose: 50 mg, temperature: 303–323 K).

(303–323 K). From the results, it was observed that the adsorbed amount of both dyes raised with equilibrium time up to 120 min at all temperatures, after that the adsorption remained at a constant level. The initial sharp rise in the adsorption efficiencies may be due to the sufficient number of available active sites on the AASP surface. The adsorption efficiency decreases with further increase in the contact time because the active adsorption sites on the adsorbent surface are unavailable. Thus, the optimal equilibrium time was 120 min.

Adsorption kinetics

Adsorption kinetic study is essential in investigating the adsorption mechanism, which is necessary to evaluate the dye uptake efficiency. In order to examine the rate of adsorption of AY 17 and AMR onto AASP, two different kinetic models were used, pseudo-first-order (Lagergren 1898), and pseudo-second-order (Ho and McKay 1999). The following equations generally express the non-linear forms of the kinetic (PFO and PSO) models.

$$q_t = q_{e1}(1 - \exp(-k_1t)) \quad (5)$$

$$q_t = \frac{q_{e2}^2 k_2 t}{1 + q_{e2} k_2 t} \quad (6)$$

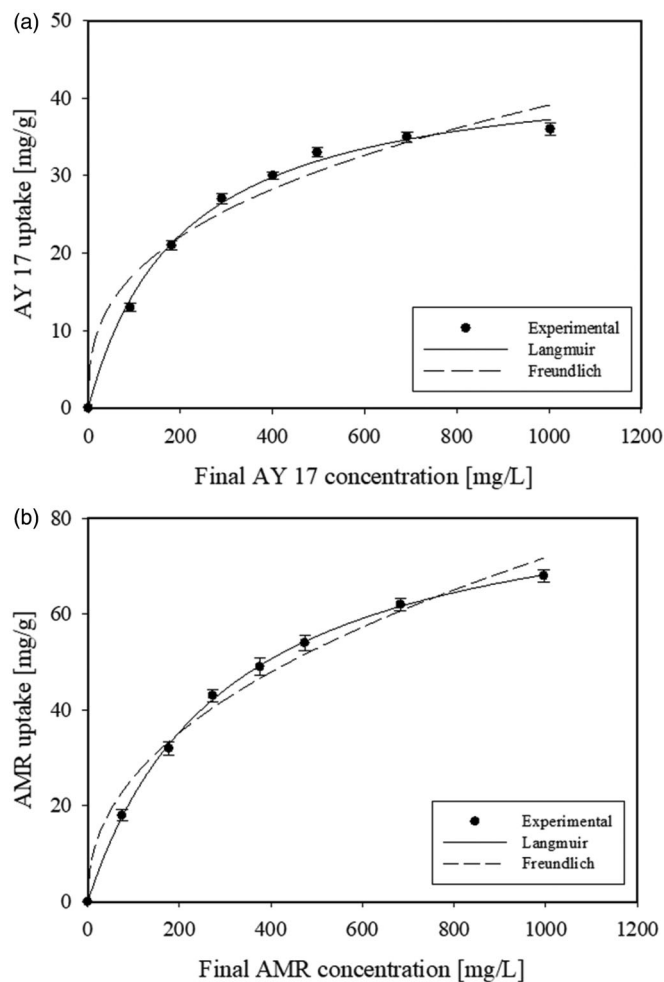
**Figure 7.** Non-linear isotherm plots for the adsorption of (a) AY 17; and (b) AMR onto AASP (initial dye concentration: 100–1,000 mg/L, volume: 30 mL, agitation: 180 rpm, pH: 2.0, dose: 50 mg, time: 120 min, temperature: 303 K).

Figure 5a,b shows PFO and PSO kinetic plots for AY 17 and AMR adsorption onto AASP at different temperatures. The relative kinetic parameters of the PFO and PSO models (obtained from the non-linear regression method) are presented in Table 2. Considering the regression coefficient (R^2), the best correlation of experimental data was with the PSO kinetic model data of AY 17 and AMR. Also, the calculated q_{e2} values from PSO model were closer to the experimental q_e values, suggesting that the electrostatic interactions nature between AASP, and dye (AY 17 and AMR). Particularly positively charged amine groups in AASP, and the negatively charged

sulfonate groups in the AY 17 and AMR, boost the adsorption process.

Adsorption activation energy

The Arrhenius equation is used to correlate the activation energy (E_a) and the rate constant of the PSO model at three different temperatures. This equation can be expressed as follows:

$$\ln k_2 = \ln A_o - \frac{E_a}{RT} \quad (7)$$

The magnitude of the E_a could be used to determine the type of adsorption process, either physisorption or chemisorption. The physisorption energy requirements are smaller (5–40 kJ/mol), reversible and equilibrium is rapidly attained. The chemisorption reactions involve stronger forces and thus requiring higher activation energies (40–800 kJ/mol) (Banerjee *et al.* 2015; Koyuncu and Okur 2021). E_a can be calculated from the slope of a linear plot between $\ln k_2$ and $1/T$ (Figure 6). The computed value of E_a for the adsorption of AY 17 and AMR on the AASP was found to be 19.9 and 15.9 kJ/mol, respectively, suggesting that the physisorption was the predominant mechanism involved.

Table 3. Isotherm parameters for the adsorption of AY 17 and AMR onto AASP.

Dye	Isotherm	Parameters	Values
AY 17	Langmuir	q_m (mg/g)	42.7 ± 1.3
		K_L (L/mg)	0.0051 ± 0.0004
		R^2	0.9971
	Freundlich	χ^2	5.4
		K_f (mg/g)	3.384 ± 1.075
		n	2.823 ± 0.412
AMR	Langmuir	R^2	0.9466
		χ^2	21.2
		q_m (mg/g)	89.2 ± 1.13
	Freundlich	K_L (L/mg)	0.0033 ± 0.0001
		R^2	0.9995
		χ^2	2.9
AY 17	Langmuir	K_f (mg/g)	3.468 ± 0.823
		n	2.261 ± 0.2
		R^2	0.9741
	Freundlich	χ^2	16.4

Table 4. Comparison of the adsorption capacities of different adsorbents for the removal of AY 17 and AMR from aqueous media.

Dye	Adsorbent	q_{max} (mg/g)	Reference	
AMR	Water hyacinth leaves	70.61	(Guerrero-Coronilla <i>et al.</i> 2015)	
	Fe ₃ O ₄ /MgO nanoparticles	38.1	(Salem <i>et al.</i> 2016)	
	PPY-CS-LS	29.5	(Zhou <i>et al.</i> 2017)	
	LMSH/NIPAm	1.58	(Bai <i>et al.</i> 2016)	
	Layered double hydroxides	0.967	(Abdellaoui <i>et al.</i> 2017)	
	Fe ₃ O ₄ @mZnO ₂ /rGO	76.90	(Jiang <i>et al.</i> 2014)	
	Alumina reinforced polystyrene	20.2	(Ahmad and Kumar 2011)	
	Aminated avocado seed powder	89.2	Present study	
	AY 17	AC/ α -Fe ₂ O ₃ composite	71.43	(Ranjithkumar, Sangeetha, <i>et al.</i> 2014)
		Silica nanofibre	40.32	(Teli and Nadathur 2018)
Commercial activated carbon		83.33	(Ranjithkumar, Nizarul Hazeen, <i>et al.</i> 2014)	
Non-living aerobic granular sludge		133.3	(Gao <i>et al.</i> 2010)	
TiO ₂ and corn cob film		0.241	(Gan <i>et al.</i> 2017)	
	Aminated avocado seed powder	42.7	Present study	

Adsorption isotherms

The adsorption isotherms are the graphical curves at a constant temperature that shows the relation between the amount of dye adsorbed and the remaining dye concentration in the equilibrium solution. To estimate the total amount of sorbent required to remove the adsorbate from the solution the isotherms are essential. In the present study, two well-known non-linear models Langmuir (Langmuir 1918), and Freundlich (Freundlich 1906) was used to analyzing the experimental equilibrium data of AY 17 and AMR adsorption.

The Langmuir isotherm describes the monolayer exposure of the adsorbate on a homogeneous surface with no interactions between the adsorbed molecules. The Langmuir model estimates the maximum uptake of the adsorption process. It can be expressed by Equation (8):

$$q_e = \frac{q_{max} K_L C_e}{1 + K_L C_e} \quad (8)$$

The maximum sorption capacities (q_{max}) of the AASP were found to be 42.7 mg/g, and 89.2 mg/g for AY 17 and AMR, respectively. The nature of adsorption was calculated by a dimensionless constant known as separation factor (R_L), expressed by the following Equation (9):

$$R_L = \frac{1}{1 + K_L C_o} \quad (9)$$

The value of R_L indicate the type of adsorption process: $R_L > 1$ (unfavorable), $R_L = 0$ (irreversible), $0 < R_L < 1$ (favorable), and $R_L = 1$ (linear). In this work, the calculated R_L values were found to be 0.363 and 0.457 for AY 17 and AMR, respectively, which indicates that the adsorption process is favorable for the evaluated AASP.

Freundlich model depends on the theory of heterogeneous surfaces with unequal energies are available on the adsorbent surface for adsorption. It is represented in Equation (10):

$$q_e = K_f C_e^{1/n} \quad (10)$$

If the n value is in the range from 1 to 10, the adsorption is said to be favorable (Munagapati *et al.* 2019). In the present study, the n value obtained from Freundlich model for AY 17 and AMR was found to be 2.823, and 2.261,

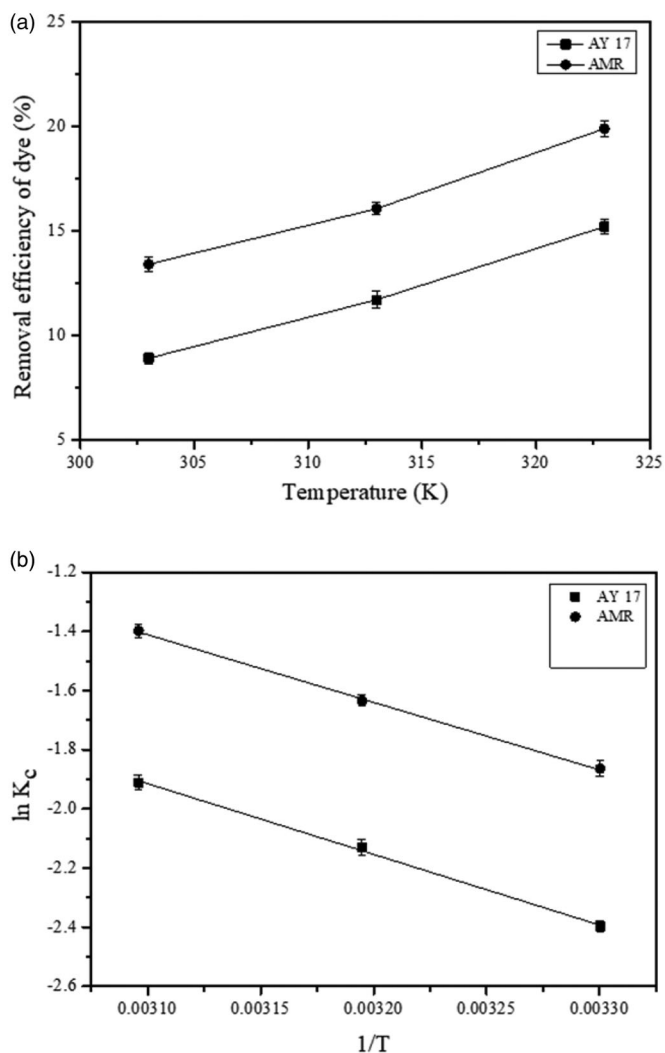


Figure 8. (a) Effect of temperature; and (b) plots of $\ln K_c$ versus $1/T$ on the adsorption of AY 17 and AMR onto AASP (initial dye concentration: 300 mg/L, volume: 30 mL, agitation: 180 rpm, pH: 2.0, dose: 50 mg, time: 120 min, temperature: 303–323 K).

Table 5. Thermodynamic parameters for the adsorption of AY 17 and AMR onto AASP.

Dye	Temp. (K)	ΔG° (kJ/mol)	ΔS° (kJ/mol K)	ΔH° (kJ/mol)
AY 17	303	6.038 ± 0.689	0.045 ± 0.001	19.79 ± 0.91
	313	5.540 ± 0.574		
	323	5.132 ± 0.516		
AMR	303	4.696 ± 0.398	0.047 ± 0.001	18.94 ± 0.69
	313	4.252 ± 0.343		
	323	3.754 ± 0.218		

respectively, indicating the adsorption of AY 17 and AMR onto AASP is favorable.

Figure 7a,b and Table 3 displayed the non-linear plots and the estimated equilibrium parameters for the removal of AY 17 and AMR onto AASP, respectively. Based on the higher value of the R^2 and lower value of χ^2 , it is clear that the Langmuir isotherm model was the most adequate to represent the adsorption equilibrium of AY 17 and AMR.

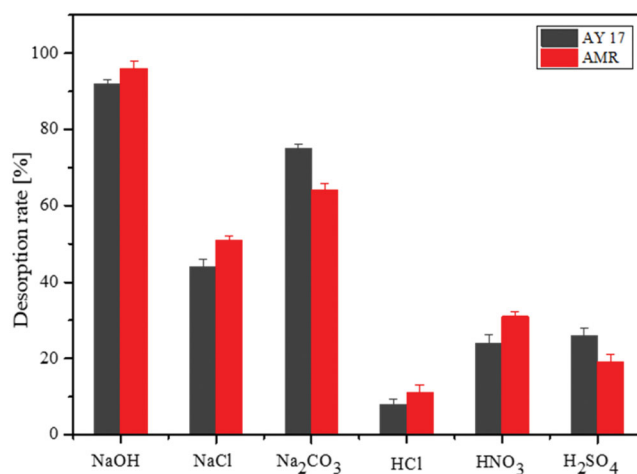


Figure 9. Desorption of AY 17 and AMR from the AASP using different eluents.

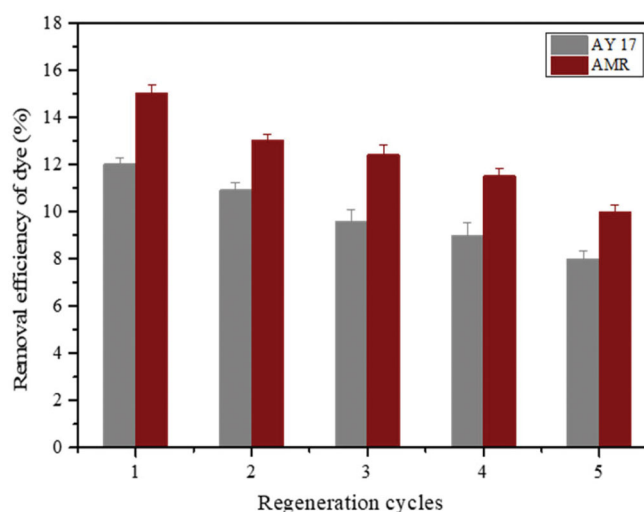


Figure 10. Adsorption-desorption cycles for (a) AY 17; and (b) AMR using 0.1 M NaOH eluent.

Comparison of AASP with other adsorbents for removal of AY 17 and AMR

The adsorption efficiency of AASP obtained in the present work for adsorption of AY 17 and AMR was compared with various adsorbents that have been reported in the literature (Table 4). From Table 4, it was noted that AASP has a satisfactory adsorption efficiency comparison with other adsorbents. So, AASP can be an efficient, suitable adsorbent for the adsorption of AY 17 and AMR from the aqueous environments.

Effect of temperature

The effect of temperature on the sorption of AY 17 and AMR onto AASP shown in Figure 8a. The experiments carried out at various temperatures (303, 313, and 323 K) at a constant initial dyes concentration of 300 mg/L, and a pH of 2.0. As shown in Figure 8a, the AASP adsorption efficiency toward AY 17 and AMR gradually increased from 9.2% to 15.2%, and from 13.4% to 19.89%, respectively when temperature raised from 303 to 323 K. When the temperature

increased, the mobility of the dye ion also increases. Therefore, a number of molecules acquiring sufficient energy to undertake an interaction with the active site at the surface also increases; as a result, adsorption increases. So, the adsorption of AY 17 and AMR on the surface of AASP is the endothermic nature of the sorption process. The thermodynamic parameters (ΔG° , ΔH° , and ΔS°) were used to define the thermodynamic behavior of the adsorption of AY 17 and AMR onto AASP. The following Equations (11–14) determined the thermodynamic parameters:

$$\Delta G^\circ = -RT \ln K_c \quad (11)$$

$$K_c = \frac{C_{Ae}}{C_e} \quad (12)$$

$$\Delta G^\circ = \Delta H^\circ - T \Delta S^\circ \quad (13)$$

$$\ln K_c = -\frac{\Delta G^\circ}{RT} = -\frac{\Delta H^\circ}{RT} + \frac{\Delta S^\circ}{R} \quad (14)$$

The ΔH° and ΔS° of adsorption were calculated from the slope and intercept of the Van't Hoff plots of $\ln K_c$ against $1/T$ (Figure 8b), respectively. The decreased ΔG° value with the temperature rise indicated that the adsorption is a non-spontaneous process and therefore involves an external source of energy to take place the process (Guerrero-Coronilla *et al.* 2015). The positive values of ΔH° using AASP represented endothermic nature of adsorption process for both dyes. The magnitude of ΔH° determines the type of adsorption. The heat of chemisorption falls into a range of 80–200 kJ/mol. But the heat evolved during physisorption is of the same order to the heat of condensation, *i.e.*, 2.1–20.9 kJ/mol. (Cho *et al.* 2015). Therefore, based on the values of ΔH° , the adsorption of AY 17 and AMR onto AASP may involve physisorption. The positive ΔS° values for AY 17 and AMR implied an increased extent of randomness at the AASP adsorbent-dye solution interface during the sorption. The values of all calculated thermodynamic parameters are listed in Table 5.

Desorption and reusability studies

The desorption experiments can estimate the recovery possibility of dye that is adsorbed on the adsorbent surface. The desorption of AY 17 and AMR loaded AASP was carried out using 0.1 M NaOH, NaCl, Na_2CO_3 , HCl, HNO_3 , and H_2SO_4 solutions. The eluting efficiency of different solutions is illustrated in Figure 9. The results suggested that 0.1 M NaOH exhibited the highest desorption efficiency of 92% and 96% for AY 17 and AMR, respectively. Hence, the regeneration studies were performed using 0.1 M NaOH eluent for five consecutive adsorption-desorption cycles, and the results were shown in Figure 10. The AASP maintained 12% and 15% removal efficiencies for AY 17 and AMR respectively after one adsorption-desorption cycle. After five cycles of reuse, the regenerated AASP still retained about 8% and 10% removal efficiencies for AY 17 and AMR respectively. The AY 17 and AMR removal efficiency of

AASP decreased with increasing cycle number. However, the decrease of adsorption efficiency could be caused by the loss of active sites, incomplete desorption and weak electrostatic attractions between the adsorbent and the adsorbate. Thus, the obtained results demonstrated that the AASP could be efficiently reused up to five cycles for the removal of AY 17 and AMR from aqueous solutions without much loss of adsorption efficiency.

Conclusions

The removal of AY 17 and AMR from the aqueous medium was studied using AASP as adsorbent. Prepared AASP (before and after dye adsorption) was characterized through FTIR, FESEM, EDX, and N_2 adsorption/desorption analysis. The AY 17 and AMR dyes are involved in electrostatic interactions with the surface of the AASP. The kinetic parameters of the adsorption process were evaluated by using non-linear PFO and PSO modes at different temperatures. Adsorption kinetics of AY 17 and AMR onto AASP followed the PSO model. The E_a was calculated at 19.9 and 15.2 kJ/mol from the Arrhenius equation, which indicated that the adsorption process of AY 17 and AMR onto AASP involves physisorption. Non-linear isotherm models (Langmuir and Freundlich) were used to analyze the equilibrium adsorption data. Based on low χ^2 and high R^2 values, the Langmuir model better described the sorption process. The adsorption of AY 17 and AMR strongly depended on the pH solution and maximum adsorption capacity of AY 17 (42.7 mg/g), and AMR (89.2 mg/g) was observed at pH 2.0. The pH at the pH_{pzc} of AASP was found to be 5.8. The thermodynamic results (ΔG° , ΔS° , and ΔH°) demonstrated that the adsorption of AY 17 and AMR are non-spontaneous and endothermic in the temperature range 303–323 K. Desorption studies showed that 0.1 M NaOH was the best desorbing eluent which desorbed 92% and 96% of AY 17 and AMR, respectively. The reusability potential of AASP for the removal of AY 17 and AMR was confirmed from the adsorption/desorption experiments with negligible activity loss even after five cycles. The obtained results suggest that the AASP can be successfully employed for the removal of AY 17 and AMR from an aqueous medium.

Nomenclature

A_o	frequency factor
BET	Brunauer-Emmett-Teller
BJH	Barret-Joyner-Halenda
C_e	equilibrium concentration of dye solution, mg/L
C_o	initial concentration of dye solution, mg/L
C_{Ae}	solid phase concentration at equilibrium, mg/L
E_a	Arrhenius activation energy, kJ/mol
EDX	Energy Dispersive X-ray spectroscopy
FT-IR	Fourier Transform Infrared Spectroscopy
k_1	PFO rate constant, 1/min
k_2	PSO rate constant, g/mg min
K_c	equilibrium adsorption distribution coefficient
K_f	Freundlich constant related to adsorption capacity, mg/g
K_L	Langmuir constant, L/mg
M	mass of adsorbent used, g
n	number of data points (χ^2 analysis)

n	Freundlich constant (dimensionless)
$1/n$	heterogeneity factor
PFO	pseudo-first-order
PSO	pseudo-second-order
q_e	amount of the dye adsorbed at equilibrium, mg/g
$q_{e,cal}$	equilibrium capacity obtained by calculated from model, mg/g
$q_{e,exp}$	equilibrium capacity from the experimental data, mg/g
q_{e1}, q_{e2}	amount of dye adsorbed at equilibrium, mg/g
q_t	amount of dye adsorbed at time t, mg/g
q_{max}	saturated monolayer adsorption capacity of the adsorbent, mg/g
R	ideal gas constant, 8.314 J/mol K
FE-SEM	Field Emission Scanning Electron Microscopy
T	absolute temperature, K
V	volume of dye solution, L
ΔG°	change in Gibbs free energy, kJ/mol
ΔH°	change in enthalpy, kJ/mol
ΔS°	change in entropy, kJ/mol K

Funding

The authors would like to acknowledge the research support from MOST 106-2625-M-224-002, MOST 106-2915-I-224-501, MOST 107-2625-M-224-002, and MOST 108-2625-M-224-005, by the Minister of Science and Technology (MOST), Taiwan.

References

- Abdellaoui K, Pavlovic I, Bouhent M, Benhamou A, Barriga C. 2017. A comparative study of the amaranth azo dye adsorption/desorption from aqueous solutions by layered double hydroxides. *Appl Clay Sci.* 143:142–150. doi:10.1016/j.clay.2017.03.019.
- Adeyemo AA, Adeoye IO, Bello OS. 2017. Adsorption of dyes using different types of clay: a review. *Appl Water Sci.* 7(2):543–568. doi:10.1007/s13201-015-0322-y.
- Ahmad R, Kumar R. 2011. Adsorption of amaranth dye onto alumina reinforced polystyrene. *Clean Soil Air Water.* 39(1):74–82. doi:10.1002/clen.201000125.
- Albadarin AB, Mo J, Glocheux Y, Allen S, Walker G, Mangwandi C. 2014. Preliminary investigation of mixed adsorbents for the removal of copper and methylene blue from aqueous solutions. *Chem Eng J.* 255:525–534. doi:10.1016/j.cej.2014.06.029.
- Ashraf MA, Hussain M, Mahmood K, Wajid A, Yusof M, Alias Y, Yusoff I. 2013. Removal of acid yellow-17 dye from aqueous solution using eco-friendly biosorbent. *Desalin Water Treat.* 51(22–24):4530–4545. doi:10.1080/19443994.2012.747187.
- Bai H, Zhang Q, He T, Zheng G, Zhang G, Zheng L, Ma S. 2016. Adsorption dynamics, diffusion and isotherm models of poly(NIPAm/LMSH) nanocomposite hydrogels for the removal of anionic dye Amaranth from an aqueous solution. *Appl Clay Sci.* 124–125:157–166. doi:10.1016/j.clay.2016.02.007.
- Banerjee S, Dubey S, Gautam RK, Chattopadhyaya MC, Sharma YC. 2019. Adsorption characteristics of alumina nanoparticles for the removal of hazardous dye, Orange G from aqueous solutions. *Arab J Chem.* 12(8):5339–5354. doi:10.1016/j.arabjc.2016.12.016.
- Banerjee S, Gautam RK, Jaiswal A, Chattopadhyaya MC, Sharma YC. 2015. Rapid scavenging of methylene blue dye from a liquid phase by adsorption on alumina nanoparticles. *RSC Adv.* 5(19):14425–14440. doi:10.1039/C4RA12235F.
- Benkaddour S, Slimani R, Hiyane H, El Ouahabi I, Hachoumi I, El Antri S, Lazar S. 2018. Removal of reactive yellow 145 by adsorption onto treated watermelon seeds: kinetic and isotherm studies. *Sustain Chem Pharm.* 10:16–21. doi:10.1016/j.scp.2018.08.003.
- Bhomick PC, Supong A, Baruah M, Pongener C, Sinha D. 2018. Pine Cone biomass as an efficient precursor for the synthesis of activated biocarbon for adsorption of anionic dye from aqueous solution: isotherm, kinetic, thermodynamic and regeneration studies. *Sustain Chem Pharm.* 10:41–49. doi:10.1016/j.scp.2018.09.001.
- Çelekli A, Al-Nuaimi AI, Bozkurt H. 2019. Adsorption kinetic and isotherms of Reactive Red 120 on *Moringa oleifera* seed as an eco-friendly process. *J Mol Struct.* 1195:168–178. doi:10.1016/j.molstruc.2019.05.106.
- Çelekli A, Ilgün G, Bozkurt H. 2012. Sorption equilibrium, kinetic, thermodynamic, and desorption studies of Reactive Red 120 on *Chara contraria*. *Chem Eng J.* 191:228–235. doi:10.1016/j.cej.2012.03.007.
- Chen H, Zhao J, Wu J, Dai G. 2011. Isotherm, thermodynamic, kinetics and adsorption mechanism studies of methyl orange by surfactant modified silkworm exuviae. *J Hazard Mater.* 192(1):246–254. doi:10.1016/j.jhazmat.2011.05.014.
- Cho E, Tahir MN, Kim H, Yu JH, Jung S. 2015. Removal of methyl violet dye by adsorption onto N-benzyltriazole derivatized dextran. *RSC Adv.* 5(43):34327–34334. doi:10.1039/C5RA03317A.
- Freundlich HMF. 1906. Über die adsorption in lasugen. *J Phys Chem.* 57:385–470.
- Gan HY, Leow LE, Ong ST. 2017. Utilization of corn cob and TiO₂ photocatalyst thin films for dyes removal. *Acta Chim Slov.* 64(1):144–158. doi:10.17344/acsi.2016.2983.
- Gao J, Zhang Q, Su K, Chen R, Peng Y. 2010. Biosorption of Acid Yellow 17 from aqueous solution by non-living aerobic granular sludge. *J Hazard Mater.* 174(1–3):215–225. doi:10.1016/j.jhazmat.2009.09.039.
- Guediri A, Bouguettoucha A, Chebli D, Chafai N, Amrane A. 2020. Molecular dynamic simulation and DFT computational studies on the adsorption performances of methylene blue in aqueous solutions by orange peel-modified phosphoric acid. *J Mol Struct.* 1202:127290. doi:10.1016/j.molstruc.2019.127290.
- Guerrero-Coronilla I, Morales-Barrera L, Cristiani-Urbina E. 2015. Kinetic, isotherm and thermodynamic studies of amaranth dye biosorption from aqueous solution onto water hyacinth leaves. *J Environ Manage.* 152:99–108. doi:10.1016/j.jenvman.2015.01.026.
- Gündüz F, Bayrak B. 2017. Biosorption of malachite green from an aqueous solution using pomegranate peel: equilibrium modelling, kinetic and thermodynamic studies. *J Mol Liq.* 243:790–798. doi:10.1016/j.molliq.2017.08.095.
- Hamza W, Dammak N, Hadjiltaief HB, Eloussaief M, Benzina M. 2018. Sono-assisted adsorption of crystal violet dye onto tunisian smectite clay: characterization, kinetics and adsorption isotherms. *Ecotoxicol Environ Saf.* 163:365–371. doi:10.1016/j.ecoenv.2018.07.021.
- Hassan W, Noureen S, Mustaqem M, Saleh TA, Zafar S. 2020. Efficient adsorbent derived from *Haloxylon recurvum* Plant for the adsorption of Acid Brown dye: kinetics, isotherm and thermodynamic optimization. *Surf Interfaces.* 20:100510. doi:10.1016/j.surf.2020.100510.
- Ho YS, McKay G. 1999. Pseudo-second order model for sorption processes. *Process Biochem.* 34(5):451–465. doi:10.1016/S0032-9592(98)00112-5.
- Jiang H, Chen P, Zhang W, Luo S, Luo X, Au C, Li M. 2014. Deposition of nano Fe₃O₄@mZrO₂ onto exfoliated graphite oxide sheets and its application for removal of amaranth. *Appl Surf Sci.* 317:1080–1089. doi:10.1016/j.apsusc.2014.09.023.
- Jiang Z, Hu D. 2019. Molecular mechanism of anionic dyes adsorption on cationized rice husk cellulose from agricultural wastes. *J Mol Liq.* 276:105–114. doi:10.1016/j.molliq.2018.11.153.
- Kamranifar M, Khodadadi M, Samiei V, Dehdashti B, Noori Sepehr M, Rafati L, Nasseh N. 2018. Comparison the removal of reactive red 195 dye using powder and ash of barberry stem as a low cost adsorbent from aqueous solutions: isotherm and kinetic study. *J Mol Liq.* 255:572–577. doi:10.1016/j.molliq.2018.01.188.
- Koyuncu DDE, Okur M. 2021. Removal of AV 90 dye using ordered mesoporous carbon materials prepared via nanocasting of KIT-6: adsorption isotherms, kinetics and thermodynamic analysis. *Sep Purif Technol.* 257:117657. doi:10.1016/j.seppur.2020.117657.
- Kumar PS, Ramalingam S, Senthamarai C, Niranjana M, Vijayalakshmi P, Sivanesan S. 2010. Adsorption of dye from aqueous solution by cashew nut shell: studies on equilibrium isotherm,

- kinetics and thermodynamics of interactions. *Desalination*. 261(1–2): 52–60. doi:10.1016/j.desal.2010.05.032.
- Lagergren S. 1898. About the theory of so-called adsorption of soluble substances. *K Sven Vetenskapsakad Handl.* 24:1–39.
- Langmuir I. 1918. The adsorption of gases on plane surfaces of glass, mica and platinum. *J Am Chem Soc.* 40(9):1361–1403. doi:10.1021/ja02242a004.
- Li B, Dong Y, Zou C, Xu Y. 2014. Iron(III)-alginate fiber complex as a highly effective and stable heterogeneous fenton photocatalyst for mineralization of organic dye. *Ind Eng Chem Res.* 53(11): 4199–4206. doi:10.1021/ie404241r.
- Liao H, Wang Z. 2018. Adsorption removal of amaranth by nanoparticles-composed Cu₂O microspheres. *J Alloys Compd.* 769: 1088–1095. doi:10.1016/j.jallcom.2018.08.088.
- Ma A, Abushaikh A, Allen SJ, McKay G. 2019. Ion exchange homogeneous surface diffusion modelling by binary site resin for the removal of nickel ions from wastewater in fixed beds. *Chem Eng J.* 358:1–10. doi:10.1016/j.cej.2018.09.135.
- Mahmoud ME, Abdelfattah AM, Tharwat RM, Nabil GM. 2020. Adsorption of negatively charged food tartrazine and sunset yellow dyes onto positively charged triethylenetetramine biochar: optimization, kinetics and thermodynamic study. *J Mol Liq.* 318:114297. doi: 10.1016/j.molliq.2020.114297.
- Mashkoo F, Nasar A. 2019. Preparation, characterization and adsorption studies of the chemically modified *Luffa aegyptica* peel as a potential adsorbent for the removal of malachite green from aqueous solution. *J Mol Liq.* 274:315–327. doi:10.1016/j.molliq.2018.10.119.
- Munagapati VS, Kim DS. 2016. Adsorption of anionic azo dye Congo Red from aqueous solution by cationic modified orange peel powder. *J Mol Liq.* 220:540–548. doi:10.1016/j.molliq.2016.04.119.
- Munagapati VS, Wen JC, Pan CL, Gutha Y, Wen JH. 2019. Enhanced adsorption performance of Reactive Red 120 azo dye from aqueous solution using quaternary amine modified orange peel powder. *J Mol Liq.* 285:375–385. doi:10.1016/j.molliq.2019.04.081.
- Munagapati VS, Wen JC, Pan CL, Gutha Y, Wen JH, Mallikarjuna Reddy G. 2020. Adsorptive removal of anionic dye (Reactive Black 5) from aqueous solution using chemically modified banana peel powder: kinetic, isotherm, thermodynamic, and reusability studies. *Int J Phytorem.* 22(3):267–278. doi:10.1080/15226514.2019.1658709.
- Munagapati VS, Yarramuthi V, Kim Y, Lee KM, Kim DS. 2018. Removal of anionic dyes (Reactive Black 5 and Congo Red) from aqueous solutions using Banana Peel Powder as an adsorbent. *Ecotoxicol Environ Saf.* 148:601–607. doi:10.1016/j.ecoenv.2017.10.075.
- Nidheesh PV, Zhou M, Oturan MA. 2018. An overview on the removal of synthetic dyes from water by electrochemical advanced oxidation processes. *Chemosphere.* 197:210–227. doi:10.1016/j.chemosphere.2017.12.195.
- Njoku VO, Foo KY, Asif M, Hameed BH. 2014. Preparation of activated carbons from rambutan (*Nephelium lappaceum*) peel by microwave-induced KOH activation for acid yellow 17 dye adsorption. *Chem Eng J.* 250:198–204. doi:10.1016/j.cej.2014.03.115.
- Qi Y, Zhu L, Shen X, Sotto A, Gao C, Shen J. 2019. Polyethyleneimine-modified original positive charged nanofiltration membrane: removal of heavy metal ions and dyes. *Sep Purif Technol.* 222: 117–124. doi:10.1016/j.seppur.2019.03.083.
- Ranjithkumar V, Nizarul Hazeen A, Thamilselvan M, Vairam S. 2014. Magnetic activated carbon-Fe₃O₄ nanocomposites-synthesis and applications in the removal of acid yellow dye 17 from water. *J Nanosci Nanotechnol.* 14(7):4949–4958. doi:10.1166/jnn.2014.9068.
- Ranjithkumar V, Sangeetha S, Vairam S. 2014. Synthesis of magnetic activated carbon/ α -Fe₂O₃ nanocomposite and its application in the removal of acid yellow 17 dye from water. *J Hazard Mater.* 273: 127–135. doi:10.1016/j.jhazmat.2014.03.034.
- Roşu M-C, Socaci C, Floare-Avram V, Borodi G, Pogăcean F, Coroş M, Măgeruşan L, Pruneanu S. 2016. Photocatalytic performance of graphene/TiO₂-Ag composites on amaranth dye degradation. *Mater Chem Phys.* 179:232–241. doi:10.1016/j.matchemphys.2016.05.035.
- Salem ANM, Ahmed MA, El-Shahat MF. 2016. Selective adsorption of amaranth dye on Fe₃O₄/MgO nanoparticles. *J Mol Liq.* 219:780–788. doi:10.1016/j.molliq.2016.03.084.
- Saritha V, Srinivas N, Srikanth Vuppala NV. 2017. Analysis and optimization of coagulation and flocculation process. *Appl Water Sci.* 7(1):451–460. doi:10.1007/s13201-014-0262-y.
- Senthil Kumar P, Fernando PSA, Ahmed RT, Srinath R, Priyadarshini M, Vignesh AM, Thanjiappan A. 2014. Effect of temperature on the adsorption of methylene blue dye onto sulfuric acid-treated orange peel. *Chem Eng Commun.* 201(11):1526–1547. doi:10.1080/00986445.2013.819352.
- Siddiqui SI, Rathi G, Chaudhry SA. 2018. Acid washed black cumin seed powder preparation for adsorption of methylene blue dye from aqueous solution: thermodynamic, kinetic and isotherm studies. *J Mol Liq.* 264:275–284. doi:10.1016/j.molliq.2018.05.065.
- Silva LS, Lima LCB, Silva FC, Matos JME, Santos MRMC, Santos Júnior LS, Sousa KS, da Silva Filho EC. 2013. Dye anionic sorption in aqueous solution onto a cellulose surface chemically modified with aminoethanethiol. *Chem Eng J.* 218:89–98. doi:10.1016/j.cej.2012.11.118.
- Stavrinou A, Aggelopoulos CA, Tsakiroglou CD. 2018. Exploring the adsorption mechanisms of cationic and anionic dyes onto agricultural waste peels of banana, cucumber and potato: adsorption kinetics and equilibrium isotherms as a tool. *J Environ Chem Eng.* 6(6): 6958–6970. doi:10.1016/j.jece.2018.10.063.
- Subbaiah MV, Kim DS. 2016. Adsorption of methyl orange from aqueous solution by aminated pumpkin seed powder: kinetics, isotherms, and thermodynamic studies. *Ecotoxicol Environ Saf.* 128:109–117. doi:10.1016/j.ecoenv.2016.02.016.
- Teli MD, Nadathur GT. 2018. Adsorptive removal of acid yellow 17 (an anionic dye) from water by novel ionene chloride modified electrospun silica nanofibres. *J Environ Chem Eng.* 6(6):7257–7272. doi: 10.1016/j.jece.2018.10.005.
- Thirunavukkarasu A, Muthukumar K, Nithya R. 2018. Adsorption of acid yellow 36 onto green nanoceria and amine functionalized green nanoceria: comparative studies on kinetics, isotherm, thermodynamics, and diffusion analysis. *J Taiwan Inst Chem Eng.* 93:211–225. doi:10.1016/j.jtice.2018.07.006.
- Wong S, Tumari HH, Ngadi N, Mohamed NB, Hassan O, Mat R, Saidina Amin NA. 2019. Adsorption of anionic dyes on spent tea leaves modified with polyethyleneimine (PEI-STL). *J Clean Prod.* 206:394–406. doi:10.1016/j.jclepro.2018.09.201.
- Yaseen DA, Scholz M. 2018. Treatment of synthetic textile wastewater containing dye mixtures with microcosms. *Environ Sci Pollut Res.* 25(2):1980–1997. doi:10.1007/s11356-017-0633-7.
- Zaidi NAHM, Lim LBL, Usman A. 2019. Enhancing adsorption of malachite green dye using base-modified *Artocarpus odoratissimus* leaves as adsorbents. *Environ Technol Innov.* 13:211–223. doi:10.1016/j.eti.2018.12.002.
- Zhao Y, Zhu L, Li W, Liu J, Liu X, Huang K. 2019. Insights into enhanced adsorptive removal of Rhodamine B by different chemically modified garlic peels: comparison, kinetics, isotherms, thermodynamics and mechanism. *J Mol Liq.* 293:111516. doi:10.1016/j.molliq.2019.111516.
- Zhou J, Lü QF, Luo JJ. 2017. Efficient removal of organic dyes from aqueous solution by rapid adsorption onto polypyrrole-based composites. *J Clean Prod.* 167:739–748. doi:10.1016/j.jclepro.2017.08.196.